Focused Ultrasound Delivers Targeted Immune Cells to Metastatic Brain Tumors

Ryan Alkins[1,2], **Alison Burgess**[1], **Milan Ganguly**[1], **Giulio Francia**[4], **Robert Kerbel**[2,4], **Winfried S. Wels**[3], and **Kullervo Hynynen**[1,2]

[1]Physical Sciences Platform, Sunnybrook Research Institute, Toronto, ON Canada

[2]Medical Biophysics, University of Toronto, Toronto, ON Canada

[3]Chemotherapeutisches Forschungsinstitut Georg-Speyer-Haus, Frankfurt, Germany

[4]Biological Sciences Platform, Sunnybrook Research Institute, Toronto, ON Canada

Abstract

Natural killer (NK) cells are cytotoxic lymphocytes involved in innate immunity. NK-92, a human NK cell line, may be targeted to tumor-associated antigens in solid malignancies where it exhibits antitumor efficacy, but its clinical utility for treating brain tumors is limited by an inability to cross the blood-brain barrier (BBB). We investigated the potential for focused ultrasound (FUS) to deliver targeted NK-92 cells to the brain using a model of metastatic breast cancer. HER2-expressing human breast tumor cells were implanted into the brain of nude rats. The NK-92-scFv(FRP5)-zeta cell line expressing a chimeric HER2 antigen receptor was transfected with super-paramagnetic iron oxide nanoparticles before intravenous injection, before and following BBB-disruption using focused ultrasound (551.5 kHz focused transducer, 0.33 MPa average peak rarefaction pressure) in the presence of a microbubble contrast agent. Baseline and post-treatment 1.5T and 7T MR imaging was performed, and histology used to identify NK-92 cells post-mortem. Contrast-enhanced MRI showed reproducible and consistent BBB-disruption. 7T MR images obtained at 16 hours post-treatment revealed a significant reduction in signal indicating the presence of iron-loaded NK-92 cells at the tumor site. The average ratio of NK-92 to tumor cells was 1:100 when NK cells were present in the vasculature at the time of sonication, versus 2:1000 and 1:1000 when delivered after sonication and without BBB-disruption, respectively. Our results offer a preclinical proof-of-concept that FUS can improve the targeting of immune cell therapy of brain metastases.

Keywords

Therapeutic Ultrasound; Immune Cell Therapy; Breast Cancer; MRI

Introduction

As many as 30% of breast cancer patients develop central nervous system (CNS) metastasis (1), for which current breast cancer therapies are inadequate (2). Systemic therapies are hindered by the cerebral capillary endothelium, which is interconnected by tight junctions, forming the blood-brain barrier (BBB) (3). The BBB normally allows passage of only small

Corresponding Author: Ryan Alkins, Sunnybrook Research Institute, 2075 Bayview Ave, C713, Toronto, ON M4N 3M5, Phone: 416-480-6100 ext 89414, Fax: 416-480-4696, ralkins@sri.utoronto.ca.

The authors disclose no potential conflicts of interest.

lipophilic compounds into the CNS. Within the tumor there is a variably more permeable blood-tumor barrier (BTB), but this still significantly hinders treatment (4). Furthermore, P-glycoprotein, expressed by cerebral capillaries and tumor cells, results in the efflux of many chemotherapeutic agents that would otherwise have therapeutic activity (5). As a result, intravenously delivered agents currently have limited efficacy in the treatment of brain metastasis (2).

Breast cancers with HER2 amplification are more aggressive, have a higher risk of CNS metastasis, and poorer prognosis (5,6). The HER2 receptor is thought to be involved in signalling pathways regulating cell growth and differentiation (6). Antibodies targeted to HER2 have resulted in improved tumor control and survival in HER2 amplified breast cancers (7), while the HER2 inhibitor lapatinib has shown improved progression-free survival in advanced HER2-positive breast cancers (8). Similar targeted treatments have been investigated in pre-clinical models using natural killer (NK) cells, the cytotoxic lymphocytes involved in the innate immune response to malignant cells (9). The HER2-specific NK-92-scFv(FRP5)-zeta cell line is a human NK-92 cell line modified to express a chimeric HER2 antigen receptor (10). It has been shown to localize to extracranial HER2 amplified breast cancers in animal models and cause selective tumor cell death (10,11,12). However, neither HER2-targeted antibodies (13,14) nor NK-92 cells are able to cross the BBB to a significant extent, while lapatinib is susceptible to P-glycoprotein and breast cancer resistance protein (15).

We investigated the feasibility of delivering HER2-specific NK-92 cells to the brain with focused ultrasound (FUS) because in contrast to antibodies and inhibitors, these cells are targeted, possess direct cytolytic activity, and are unaffected by efflux channels (9). Using ultrasound bursts at sub-megahertz frequencies through the intact skull, in combination with timed intravenous (i.v.) injections of encapsulated perfluorocarbon microbubbles, the permeability of the cerebral vasculature can be non-invasively increased in targeted, focal regions (16,17). Cavitation of microbubbles under the influence of ultrasound appears to cause temporary mechanical disruption of endothelial tight junctions, and increased para- and transcellular passage of molecules from the blood into the brain (18,19). Contrast-enhanced MRI can be used to identify the regions of contrast extravasation and confirm BBB and BTB disruption (BBBD) (17). This technique has been shown to increase the penetration of a number of therapeutic agents into the brain in rodent models (20,21,22) and has recently been shown to be safe in non-human primates (23).

We examined whether HER2-specific NK-92-scFv(FRP5)-zeta cells injected intravenously could be delivered to the brain using MRI-guided FUS in a xenograft HER2-expressing breast metastasis model. By transfecting the HER2-specific NK-92 cells with superparamagnetic iron oxide (SPIO) nanoparticles, we were able to track their accumulation at the tumor site. Furthermore, we quantified the density of effector-to-tumor cells in order to confirm that the number was sufficient to successfully treat a tumor, and assessed the cytolytic function of HER2-specific NK-92 cells following exposure to ultrasound *in vivo*.

Materials and Methods

Cell Lines and Culture

Human HER2-expressing MDA-MB-231 breast tumor cells were cells were isolated from brain metastases, secondary to a primary tumor implanted in a mouse mammary fat pad, and transfected to express HER2 as previously reported (24). MDA-MB-231-HER2 cells were maintained in RPMI 1640 media supplemented with 10% fetal bovine serum (Wisent, St. Bruno, QC Canada). For implantation, cells were collected, centrifuged and resuspended in

Hanks' balanced salt solution (HBSS; Wisent) at a concentration of 10^3 cells/µl. HER2 expression was confirmed using immunocytochemistry. MDA-MB-231-HER2 cells were plated on 8 well chamber slides (Nunc, Roskilde, Denmark) for 24 hrs and then fixed with 4% paraformaldehyde for 10 min at room temperature. Cells were treated with blocking solution containing 1% donkey serum for 1 hr followed by incubation with primary rabbit anti-HER2 (Thermo Fisher Scientific, Nepean, ON Canada) overnight. Slides were washed and incubated with donkey anti-mouse Cy3 for 1 hr, and coverslipped. Fluorescent images were captured with a Zeiss Axiovert microscope.

The human cell line, NK-92 (ATCC, Manassas, VA), was virally transduced to stably express a chimeric antigen receptor specific to HER2 (10). The antigen receptor expression was confirmed by fluorescence activated cell sorter (FACS) analysis (10). HER2-specific NK-92-scFv(FRP5)-zeta cells were maintained in X-VIVO 10 medium (Lonza, Basel, Switzerland) supplemented with 5% heat- inactivated human serum (Cedarlane, Burlington, ON Canada), 0.6 mg/ml G418 (Wisent, St. Bruno, QC Canada) and 100 µg /ml IL-2 (RnD systems, Minneapolis, MN USA). Expression of CD45 was evaluated on a cell smear of targeted cells using mouse anti-human CD45 (RnD systems, Minneapolis, MN USA) and the procedures described above. Prior to use *in vivo*, HER2-specific NK-92 zeta cells were labeled with SPIO nanoparticles (diameter 10–50 nm) as MRI contrast. 100 µg Fe_3O_4 (Sigma-Aldrich, Oakville, ON Canada) was combined with Lipofectamine transfection reagent (Invitrogen, Burlington, ON Canada) for 30 min and subsequently added to 10^6 NK-92 cells in normal media for 24 hrs at 37° (11). Cells were collected, centrifuged and resuspended in sterile, physiological saline at a concentration of 10^7 cells/ml for injection *in vivo*. Transfection efficiency was estimated using light microscopy to identify SPIO nanoparticles within the cell cytoplasm.

Tumor Implantation

All procedures were approved by the Sunnybrook Research Institute Animal Care and Use Committee and conformed to the guidelines set out by the Canadian Council on Animal Care. General anesthesia was induced and maintained with isofluorane in 250–300 g male athymic nude rats (Charles River, Sherbrooke, QC Canada). A burrhole was fashioned in the skull and cells were implanted in the left frontal striatum with a Hamiton syringe guided by stereotactic frame, at a depth of 4 mm from the cortical surface. MDA-MB-231-HER2 cells were combined with a 1% agar solution at 37°C to a final density of 10^3 cells/µL, and 10 µL were injected (25). Animals underwent serial MRI imaging and the tumors treated once they had reached 1.5–2 mm in size.

MRI-guided Focused Ultrasound

In preparation for BBBD, animals were anesthetized with ketamine (90 mg/kg) and xylazine (10 mg/kg). A 22-gauge cannula was inserted into the tail vein and the head of the animal shaved and chemically depilated. Definity® ultrasound contrast (Lantheus Medical Imaging, North Billerica, MA) was prepared as directed by the manufacturer by warming to room temperature and activating in the proprietary agitator (VIALMIX®, Lantheus Medical Imaging). It was then diluted 1:10 in 0.9% saline. Animals were positioned supine on the in-house designed 3-axis positioning system (26) and fixed in place with a bite bar and lower extremity restraints. The head was coupled to a 551.5 kHz single element focused ultrasound transducer (F=0.8, R=10 cm) through a bath of degassed water and surrounded by an in-house manufactured 3×5 cm (inner dimensions) rectangular RF surface coil (Figure 1). The focal spot size for this transducer, characterized by the full-width at half maximum of the beam pressure profile, corresponded to a diameter of 3.0 mm in the axial plane (x-y plane in Figure 1) by 12.5 mm in the beam direction (z direction in Figure 1). The tumors were therefore completely encompassed by the focus.

Targeting and registration images were acquired with a 1.5T clinical MRI scanner (Signa, GE Healthcare, Milwaukee, WI). All animals underwent baseline T2- (FOV 6 cm, 128×128 matrix, slice thickness 1 mm, NEX 2, ETL 4, TR 2000 ms, TE 75ms) and T1-weighted (FOV 6 cm, 128×128 matrix, slice thickness 1 mm, NEX 6, ETL 4, TR 500, TE ~10ms) MR imaging, including a contrast enhanced (0.2 ml/kg; Omniscan, GE Healthcare, Milwaukee, WI) sequence, to identify the tumor. Following MRI and ultrasound co-registration, the computer-controlled 3-axis positioning system allowed the focal spot of the transducer to be positioned at any location within the brain. BBBD was performed (10 ms pulses, 1 Hz pulse repetition frequency, 120 s total duration) using a controller to modulate the acoustic power (0.33 MPa average estimated peak rarefaction pressure in the brain; range 0.32–0.35 MPa) (27). The estimated in-situ pressure was determined assuming 73% transmission through the rat skull (28) and an attenuation coefficient of 5.0 Np/m/MHz in brain (16) with an acoustic path length of 5 mm.

A 60 s infusion of diluted Definity® (0.2 ml/kg) was administered via the tail vein catheter simultaneously with the onset of the sonication. Post-treatment T2- and contrast-enhanced T1-weighted sequences were acquired to assess the location and degree of BBBD. To detect iron oxide-labelled cells, imaging was conducted on a 7T MRI (BioSpec 70/30 USR, Bruker BioSpin, Billerica, MA) fitted with gradient and shim insert (BGA-S, Bruker BioSpin) and using a circularly polarized rat brain RF coil (Bruker BioSpin). Both T2- (TR=3000 ms, TE=37.2 ms, flip angle=180°) and T2*-weighted (8 echo train, TR=1000 ms, TE=24 ms, flip angle=30°) sequence were performed. The change in signal intensity within the tumor on T2*-weighted images (19 ms echo) following treatment with SPIO-labelled cells, compared with pre-treatment, was quantified.

Treatment Groups

Three treatment arms received intravenous injection of 10^9 targeted NK-92 cells/m^2 body surface area (estimated from body weight), on the order of the number of cells delivered in previous phase I/II trials (29,30). Group 1 (n=4) received HER2 specific NK-92 cells but no BBBD. Group 2 (n=4) received HER2 specific NK-92 cells following BBBD. Group 3 (n=5) had HER2 specific NK-92 cells injected immediately prior to BBBD. The experimental timeline for the three treatment groups is shown in Figure 2.

Histological Analysis

Animals were sacrificed by euthanyl injection 12–16 hrs following treatment. Brains were removed, fixed in 10% neutral buffered formalin, and serial 4 μm coronal sections cut at 250 μm levels. All sections were stained with Hematoxylin & Eosin (H&E) for morphological analysis, and Prussian blue for the detection of SPIO nanoparticles (Polysciences, Inc., Warrington, USA). IHC using the polymerized reporter enzyme staining system (Vector Laboratories, Burlingame, USA) was used to detect CD45 (mouse anti-human, 1:200, R&D Systems, Minneapolis, USA), perforin (mouse anti-human, 1:10, Abcam, Cambridge, USA) and granzyme B (rabbit anti-human, 1:100, Abcam, Cambridge, USA). Sections were digitized with a Mirax Scanner (Zeiss, Germany) and analyzed using Pannoramic Viewer (v. 1.15, 3DHISTECH, Budapest, Hungary). For each animal, 4 sequential levels were analyzed by two blinded investigators. HER2-specific NK-92 cells were identified by CD45 expression and intra-cellular iron on Prussian blue histochemistry performed on serial sections at each level. Effector cells within the tumor boundary were counted and expressed as a percentage of the number of tumor cells in each section. Effector cells outside of the tumor region were ignored for this analysis. The average ratio (effector per 100 tumor cells, mean ± SEM) was then calculated for each treatment group.

Cytotoxicity Assay

Cytotoxicity assays were performed to determine the extent of MDA-MB-231-HER2 cell death achieved using differing effector-to-tumor cell ratios. 10^6 MDA-MB-231-HER2 cells were plated and maintained for 2 hrs at $37°$. Serial dilutions (10^6, 10^5, 10^4) of HER2-specific NK-92 cells were prepared in fresh medium and added to the MDA-MB-231-HER2 cell layer (corresponding to effector:tumor cell ratios of 1:1, 1:10 and 1:100). At 2 and 24 hrs, the cells were rinsed, collected and analyzed using Trypan blue cell exclusion dye. Results were expressed as the ratio of dead cells to the total number of cells counted. Similar experiments were completed after iron transfection.

Statistical Analysis

GraphPad Prism 5 (GraphPad Software, San Diego, CA) was used for statistical analysis. Student's t test was used to compare the means $\pm$ SEM of two groups and the means $\pm$ SEM of three or more groups were compared with one-way ANOVA and Tukey's post-test. Statistical significance was noted if $p < 0.05$.

Results

Prior to implantation, HER2 expression in MDA-MB-231-HER2 cells was determined to be 80% using immunohistochemistry (IHC). CD45 expression by HER2-specific NK-92 cells was found to be 100% using IHC. The average transfection efficiency of HER2-specific NK-92 cells with SPIO nanoparticle was 80% and did not affect their cytolytic function.

Representative pre- and post-treatment contrast-enhanced T1-weighted MR images are shown in Figure 3A and 3B. The degree of contrast enhancement following BBBD was relatively uniform and was double that of the tumor region prior to treatment ($34 \pm 10\%$ versus $17 \pm 8\%$, p=0.01). All animals tolerated the cell injection and BBBD without complication, and recovered from general anesthesia to their pre-treatment condition. No abnormal behavior was noted in the 16 hour interval between treatment and sacrifice. Post-treatment 7T MR imaging detected HER2-specific NK-92 cells at the tumor site in group 3 by a $-17 \pm 4\%$ change in the signal intensity versus a $14 \pm 7\%$ change in group 1 ($p < 0.001$). Representative pre- and post-treatment T2*-weighted sequences are shown in Figures 3A and 3B. The differences between other groups were not found to be statistically significant ($p > 0.05$, Figure 4C).

Following animal sacrifice, H&E stained sections were examined for tissue injury. One FUS-treated animal had a small region of erythrocyte extravasation adjacent the tumor (Figure 3C). HER2-specific NK-92 cells were counted using both CD45 expression and the presence of intracellular iron on Prussian blue stained sections, and expressed as number of effector cells per 100 tumour cells. Without BBBD, a very small number of HER2-specific NK-92 cells localized to the tumor (group 1, 0.09 ± 0.11, Figure 5), and almost equally few reached the tumor when BBBD was done prior to the injection of cells into the circulation (group 2, 0.21 ± 0.15, Figure 5). In contrast, the ratio of HER2-specific NK-92-to-tumor cells was increased five-fold when the former were circulating at the time of sonication compared to injection afterward (group 3, 0.95 ± 0.23, Figure 5). The number of effector cells accumulating in the sonicated tumors in group 3 corresponds to approximately 0.34% of the total number of cells injected. This increase was statistically significant when compared to the former two groups ($p < 0.01$, Figure 5B). There was no statistical difference between group 1 and 2. More dense accumulations of cells were observed around arterioles and venules in group 3, with an effector:tumor ratio significantly greater than the volume-averaged value (Figure 6A and 6C). Furthermore, cells were identified outside of the tumor

boundary in a number of sections in group 3 but not counted in the analysis; theoretically these cells could migrate to the tumor and contribute to a higher effector to tumor cell ratio.

We also examined whether HER2-specific NK-92 cells circulating prior to BBBD would be negatively affected by interactions with oscillating microbubbles at the ultrasound focus. Perforin and granzyme B IHC demonstrated that HER2-specific NK-92 cells retained their function following translocation into the brain. Figure 7A illustrates a targeted NK-92 cell within the tumor having released granzyme B, which can be identified within the cytoplasm of surrounding tumor cells. Perforin was similarly seen in the extra-cellular space surrounding effector cells and within the cytoplasm of tumor cells. Tumor cells undergoing apoptosis following interaction with HER2-specific NK-92 cells are seen in Figure 7A and 7B.

Cytotoxicity assays were performed to estimate whether a sufficient number of HER2-specific NK-92 cells accumulated at the tumor sites following BBBD for efficient tumor cell lysis. At the 2-hr time point there was a higher proportion of dead MDA-MB-231-HER2 cells in the 1:10 and 1:1 NK-92:tumor groups, but at 24 hrs there were no statistically significant differences between the three different starting ratios (p > 0.05, Figure 7C).

Discussion

HER2-specific immune cells have demonstrated *in vivo* efficacy against HER2-amplified extracranial tumors when injected into the blood stream (10,11,12). Intracranially, however, successful treatment has necessitated direct injection of targeted immune cells into the tumor through a burrhole in the skull (31,32). In the present study, we have demonstrated for the first time the feasibility of using MRI-guided FUS to allow intravenously injected HER2-specific NK-92 cells access to tumors in the brain. SPIO-laden effector cells were detected at the tumor site with T2*-weighted MRI in group 3. Although an average signal decrease over the tumor volume was detected, heme breakdown products from the stereotactic implantation of tumor cells may have complicated the analysis. The presence of intra-tumoral heme products in human patients could similarly interfere with the *in vivo* tracking of SPIO nanoparticle-labeled effector cells.

The order of BBBD and cell injection was found to have a significant impact on the number of HER-specific NK-92 cells reaching the tumor (Figure 5A and 5B). The exact mechanisms underlying this increase in HER2-targeted NK-92 cell accumulation in the sonicated tumor volume are unknown. Despite identical ultrasound exposures, the presence of HER2-targeted NK-92 cells in the circulation at the time of BBBD resulted in an almost five-fold increase in the ratio of effector-to-tumor cells. One possibility is that inter-endothelial clefts may be larger during the sonication, facilitating the extravasation of effector cells present during BBBD. It is uncertain whether the effect of BBBD on endothelium stimulates or inhibits diapedesis, but if priming of the endothelium was the sole mechanism responsible for effector cell extravasation at the tumor site, the order of cell injection should have made little difference. It has been previously reported that FUS stimulates the release of nitric oxide (NO) from endothelial cells *in vitro* (33,34), as well as increases the expression of caveolin-1 *in vivo* (35), and thus it is conceivable that BBBD could affect the expression of proteins involved in leukocyte adhesion. Furthermore, the interaction of ultrasound and microbubbles with the HER2-targeted NK-92 cells may play a role. Microbubbles undergoing stable cavitation are known to generate shear stresses (36,37,38), and increased fluid shear stresses have a number of *in vitro* effects on activated leukocytes including increased adhesion (39,40), deformability (41), motility (42), and transmigration (42,43). Although speculatory, it is possible that circulating HER2-specific NK-92 cells are more likely to adhere to endothelium and extravasate following exposure to fluid shear stresses

generated by microbubbles at the ultrasound focus. These *in vitro* studies typically required fluid shear stresses in the setting of an activated endothelium, and therefore from the group 2 results (where the endothelium was exposed to FUS but the HER2-specific NK-92 cells were not) the effect of BBBD on the endothelium alone is one that at least partially promotes leukocyte extravasation, either by disrupting endothelial tight junctions or through some unknown mechanism. Finally, there may be direct mechanical effects of the oscillating microbubbles on the effector cells that have yet to be elucidated.

In addition to the increased accumulation of HER2-specific NK-92 cells in group 3 tumors, dense accumulations of HER2-specific NK-92 cells around arterioles and venules in group 3 (Figure 6A and 6C). Larger vessels may have permitted greater microbubble activity (decreased bubble damping compared to capillary sized vessels, or a bubble population with a mean size closer to the resonant frequency used), or possibly was able to support larger inter-endothelial openings. Along capillaries, the effector cells were seen to line the adluminal surface, even in the absence of nearby tumor cells (Figure 6B and 6D). We did not see any of these features in group 1 or 2 animals. Of particular note in both ultrasound-treated groups is the absence of erythrocytes amongst extravasated HER2-specific NK-92 cells (there was a small region of erythrocyte extravasation adjacent the tumor absent effector cells). It is believed this is in keeping with the postulated mechanism for the increased leukocyte extravasation with BBBD. The inter-endothelial openings, only studied post-BBBD, have been shown to be on the order of tens to hundreds of nanometers, and thus much smaller than the diameter of an erythrocyte (18,44). Erythrocytes are typically dispersed with little adherence to endothelial cells in the face of fluid shear stresses (45), whereas the reverse is true for leukocytes (39–43).

Of significant concern was whether HER2-specific NK-92 cells circulating at the time of the BBBD would maintain their cytolytic function. Figure 6A and 6C show a large group of extravascular HER2-specific NK-92 cells surrounding an extra-tumoral venule. In such a vessel (outside the tumor but within the ultrasound focus), the direction of extravasation should be random, but the preferential clustering of cells toward the tumor suggests preserved bioactivity of the cells. Furthermore, perforin and granzyme B IHC provided evidence that these mediators of apoptosis were being released into the intercellular space, and a number of apoptotic cells were identified in close association with HER2-specific NK-92 cells (Figure 7A and 7B). In addition to preserved biological function, we estimated that the effector-to-target cell ratios realized would be sufficient to result in efficient tumor cell lysis (Figure 7C). Because the SPIO nanoparticle transfection efficiency was less than 100%, the calculated densities likely underestimate the actual number of HER2-specific NK-92 cells reaching the tumors.

We have demonstrated for the first time the feasibility of using targeted immune cells combined with MRI-guided FUS to treat tumors in the brain. This treatment holds significant promise as it is specific not only to the environs of the tumor, but also to the malignant cells themselves, and can be performed non-invasively under MRI guidance. Furthermore, theoretically the NK-92 cells could be re-targeted to any number of cancer-associated antigens to allow the treatment of a variety of human malignancies. Future studies will aim to show a reduction in tumor volume and an improved survival in brain metastasis-bearing rats, as these are real-world indicators of treatment success. The NK-92 cell line has already been used in early clinical trials (29,30) and with the expanding clinical testing of FUS, and also the recent demonstration of the safety and repeatability of BBBD in rhesus macaques (23), this treatment has the potential to benefit patients with brain metastasis in the foreseeable future.

Acknowledgments

References

1. Lee Y-T. Breast carcinoma: Pattern of metastasis at autopsy. J Surg Oncol. 1983; 23:175–180. [PubMed: 6345937]

2. Lin NU, Bellon JR, Winer EP. CNS Metastases in Breast Cancer. J Clin Oncol. 2004; 22:3608–3617. [PubMed: 15337811]

3. Abbott NJ, Rönnbäck L, Hansson E. Astrocyte-endothelial interactions at the blood-brain barrier. Nat Rev Neurosci. 2006; 7:41–53. [PubMed: 16371949]

4. Lockman PR, Mittapalli RK, Taskar KS, Rudraraju V, Gril B, Bohn KA, et al. Heterogeneous blood–tumor barrier permeability determines drug efficacy in experimental brain metastases of breast cancer. Clin Cancer Res. 2010; 16:5664–5678. [PubMed: 20829328]

5. Linn SC, Giaccone G, van Diest PJ, Blokhuis WM, van Der Valk P, van Kalken CK, et al. Prognostic relevance of p-glycoprotein expression in breast cancer. Ann Oncol. 1995; 6:679–685. [PubMed: 8664189]

6. Slamon DJ, Clark GM, Wong SG, Levin WJ, Ullrich A, McGuire WL. Human breast cancer: Correlation of relapse and survival with amplification of the HER2/neu oncogene. Science. 1987; 235:177–182. [PubMed: 3798106]

7. Slamon DJ, Leyland-Jones B, Shak S, Fuchs H, Paton V, Bajamonde A, et al. Use of chemotherapy plus a monoclonal antibody against HER2 for metastatic breast cancer that overexpresses HER2. N Engl J Med. 2001; 344:783–792. [PubMed: 11248153]

8. Geyer CE, Forster J, Lindquist D, Chan S, Romieu CG, Pienkowski T, et al. Lapatinib plus capecitabine for HER2-positive advanced breast cancer. N Engl J Med. 2006; 355:2733–2743. [PubMed: 17192538]

9. Smyth MJ, Hayakawa Y, Takeda K, Yagita H. New aspects of natural-killer-cell surveillance and therapy of cancer. Nat Rev Cancer. 2002; 2:850–861. [PubMed: 12415255]

10. Uherek C, Tonn T, Uherek B, Becker S, Schnierle B, Klingemanne H-G, Wels W. Retargeting of NK-cell cytolytic activity to ErbB2 expressing tumor cells results in efficient and selective tumor cell destruction. Blood. 2002; 100:1265–1273. [PubMed: 12149207]

11. Daldrup-Link HE, Meier R, Rudelius M, Piontek G, Piert M, et al. In vivo tracking of genetically engineered anti-Her2/neu directed natural killer cells to Her2/neu positive mammary tumors with magnetic resonance imaging. Eur Radiol. 2005; 15:4–13. [PubMed: 15616814]

12. Meier R, Piert M, Piontek G, Rudelius M, Oostendorp RA, Senekowitsch-Schmidtke R, et al. Tracking of [18F]FDG-labeled natural killer cells to HER2/neu-positive tumors. Nucl Med Biol. 2008; 35:579–588. [PubMed: 18589302]

13. Pestalozzi BC, Brignoli S. Trastuzumab in CSF. J Clin Oncol. 2000; 18:2350–2351.

14. Stemmler HJ, Schmitt M, Willems A, Bernhard H, Harbeck N, Heinemann V. Ratio of trastuzumab levels in serum and cerebrospinal fluid is altered in HER2-positive breast cancer patients with brain metastases and impairment of blood-brain barrier. Anticancer Drugs. 2007; 18:23–28. [PubMed: 17159499]

15. Polli JW, Humphreys JE, Harmon KA, Castellino S, O'Mara MJ, Olson KL, et al. The role of efflux and uptake transporters in [N-{3-chloro-4-[(3-fluorobenzyl)oxy]phenyl}-6-[5-({[2-(methylsulfonyl)ethyl]amino}methyl)-2-furyl]-4-quinazolinamine (GW572016, lapatinib) disposition and drug interactions. Drug Metab Dispos. 2008; 36:695–701. [PubMed: 18216274]

16. Hynynen K, McDannold N, Vykhodtseva N, Jolesz FA. Noninvasive MR imaging-guided focal opening of the blood–brain barrier in rabbits. Radiology. 2001; 220:640–646. [PubMed: 11526261]

17. McDannold N, Vykhodtseva N, Hynynen K. Use of ultrasound pulses combined with Definity® for targeted blood-brain barrier disruption: a feasibility study. Ultrasound Med Biol. 2007; 33:584–590. [PubMed: 17337109]

18. Sheikov N, McDannold N, Vykhodtseva N, Jolesz F, Hynynen K. Cellular mechanisms of the blood-brain barrier opening induced by ultrasound in presence of microbubbles. Ultrasound Med Biol. 2004; 30:979–989. [PubMed: 15313330]

19. Sheikov N, Mcdannold N, Sharma S, Hynynen K. Effect of focused ultrasound applied with an ultrasound contrast agent on the tight junctional integrity of the brain microvascular endothelium. Ultrasound Med Biol. 2008; 34:1093–1104. [PubMed: 18378064]

20. Kinoshita M, McDannold N, Jolesz FA, Hynynen K. Noninvasive localized delivery of Herceptin to the mouse brain by MRI-guided focused ultrasound-induced blood-brain barrier disruption. Proc Natl Acad Sci. 2006; 103:11719–11723. [PubMed: 16868082]

21. Liu HL, Hua MY, Chen PY, Chu PC, Pan CH, Yang HW, et al. Blood-Brain Barrier Disruption with Focused Ultrasound Enhances Delivery of Chemotherapeutic Drugs for Glioblastoma Treatment. Radiology. 2010; 255:415–425. [PubMed: 20413754]

22. Burgess A, Ayala-Grosso CA, Ganguly M, Jordão JF, Aubert I, Hynynen K. Targeted delivery of neural stem cells to the brain using MRI-guided focused ultrasound to disrupt the blood-brain barrier. PLoS One. 2011; 6:e27877. [PubMed: 22114718]

23. McDannold N, Arvanitis CD, Vykhodtseva N, Livingstone MS. (2012). Temporary disruption of the blood-brain barrier by use of ultrasound and microbubbles: safety and efficacy evaluation in rhesus macaques. Cancer Res. 2012 May 2.

24. Francia G, Man S, Lee CJ, Xu P, Mossoba ME, Emmenegger U, et al. Comparative impact of trastuzumab and cyclophosphamide on HER-2-postive human breast cancer xenografts. Clin Cancer Res. 2009; 15:6358–6366. [PubMed: 19825954]

25. Kobayashi N, Allen N, Clendenon NR, Ko LW. An improved rat brain-tumor model. J Neurosurg. 1980; 53:808–815. [PubMed: 7003068]

26. Chopra R, Curiel L, Staruch R, Morrison L, Hynynen K. An MRI-compatible system for focused ultrasound experiments in small animal models. Med Phys. 2009; 36:1867–1874. [PubMed: 19544806]

27. O'Reilly MA, Hynynen K. Blood-Brain Barrier: Real-time Feedback-controlled Focused Ultrasound Disruption by Using an Acoustic Emissions-based Controller. Radiology. 2012; 263:96–106. [PubMed: 22332065]

28. O'Reilly MA, Muller A, Hynynen K. Ultrasound Insertion Loss of Rat Parietal Bone Appears to Be Proportional to Animal Mass at Submegahertz Frequencies. Ultrasound Med Biol. 2011; 37:1930–1937. [PubMed: 21925788]

29. Tonn T, Becker S, Esser R, Schwabe D, Seifried E. Cellular immunotherapy of malignancies using the clonal natural killer cell line NK-92. J. Hematother. Stem Cell Res. 2001; 10:535–544. [PubMed: 11522236]

30. Arai S, Meagher R, Swearingen M, Myint H, Rich E, Martinson J, Klingemann H. Infusion of the allogeneic cell line NK-92 in patients with advanced renal cell cancer or melanoma: a phase I trial. Cytotherapy. 2008; 10:625–632. [PubMed: 18836917]

31. Ahmed N, Ratnayake M, Savoldo B, Perlaky L, Dotti G, Wels WS, et al. Regression of Experimental Medulloblastoma following Transfer of HER2-Specific T Cells. Cancer Res. 2007; 67:5957–5964. [PubMed: 17575166]

32. Ahmed N, Salsman VS, Kew Y, Shaffer D, Powell S, Zhang YJ, et al. HER2-specific T cells target primary glioblastoma stem cells and induce regression of autologous experimental tumors. Clin Cancer Res. 2010; 16:474–485. [PubMed: 20068073]

33. Altland OD, Dalecki D, Suchkova VN, Francis CW. Low-intensity ultrasound increases endothelial cell nitric oxide synthase activity and nitric oxide synthesis. J Thromb Haemost. 2004; 2:637–643. [PubMed: 15102020]

34. Hsu S, Huang T. Bioeffect of ultrasound on endothelial cells in vitro. Biomol Eng. 2004; 21:99–104. [PubMed: 15567103]

35. Deng J, Huang Q, Wang F, Liu Y, Wang Z, Wang Z, et al. The role of caveolin-1 in blood-brain barrier disruption induced by focused ultrasound combined with microbubbles. J Mol Neurosci. 2012; 46:677–687. [PubMed: 21861133]

36. Ward M, Wu J, Chiu JF. Ultrasound-induced cell lysis and sonoporation enhanced by contrast agents. J Acoust Soc Am. 1999; 105(5):2951–2957. [PubMed: 10335644]

37. Wu J. Shear stress in cells generated by ultrasound. Prog Biophys Mol Biol. 2007; 93:363–373. [PubMed: 16928394]

38. VanBavel E. Effects of shear stress on endothelial cells: Possible relevance for ultrasound applications. Prog Biophys Mol Biol. 2007; 93:374–383. [PubMed: 16970981]

39. Dewitz TS, Hung TC, Martin RR, McIntire LV. Mechanical trauma in leukocytes. J Lab Clin Med. 1977; 90:728–736. [PubMed: 903701]

40. Okuyama M, Kambayashi J, Sakon M, Monden M. LFA-1/ICAM-3 mediates neutrophil homotypic aggregation under fluid shear stress. J Cell Biochem. 1996; 60:550–559. [PubMed: 8707894]

41. Moazzam F, DeLano FA, Zweifach BW, Schmid-Schönbein GW. The leukocyte response to fluid stress. Proc Natl Acad Sci. 1997; 94:5338–5343. [PubMed: 9144238]

42. Kitayama J, Hidemura A, Saito H, Nagawa H. Shear stress affects migration behavior of polymorphonuclear cells arrested on endothelium. Cell Immunol. 2000 Jul 10; 203(1):39–46. [PubMed: 10915560]

43. Cinamon G, Shinder V, Alon R. Shear forces promote lymphocyte migration across vascular endothelium bearing apical chemokines. Nat Immunol. 2001; 2:515–522. [PubMed: 11376338]

44. Marty B, Larrat B, Van Landeghem M, Robic C, Robert P, Port M, et al. Dynamic study of blood-brain barrier closure after its disruption using ultrasound: a quantitative analysis. J Cereb Blood Flow Metab. 2012 [In Press].

45. Yedgar S, Koshkaryev A, Barshtein G. The red blood cell in vascular occlusion. Pathophysiol Haemost Thromb. 2002; 32:263–268. [PubMed: 13679654]
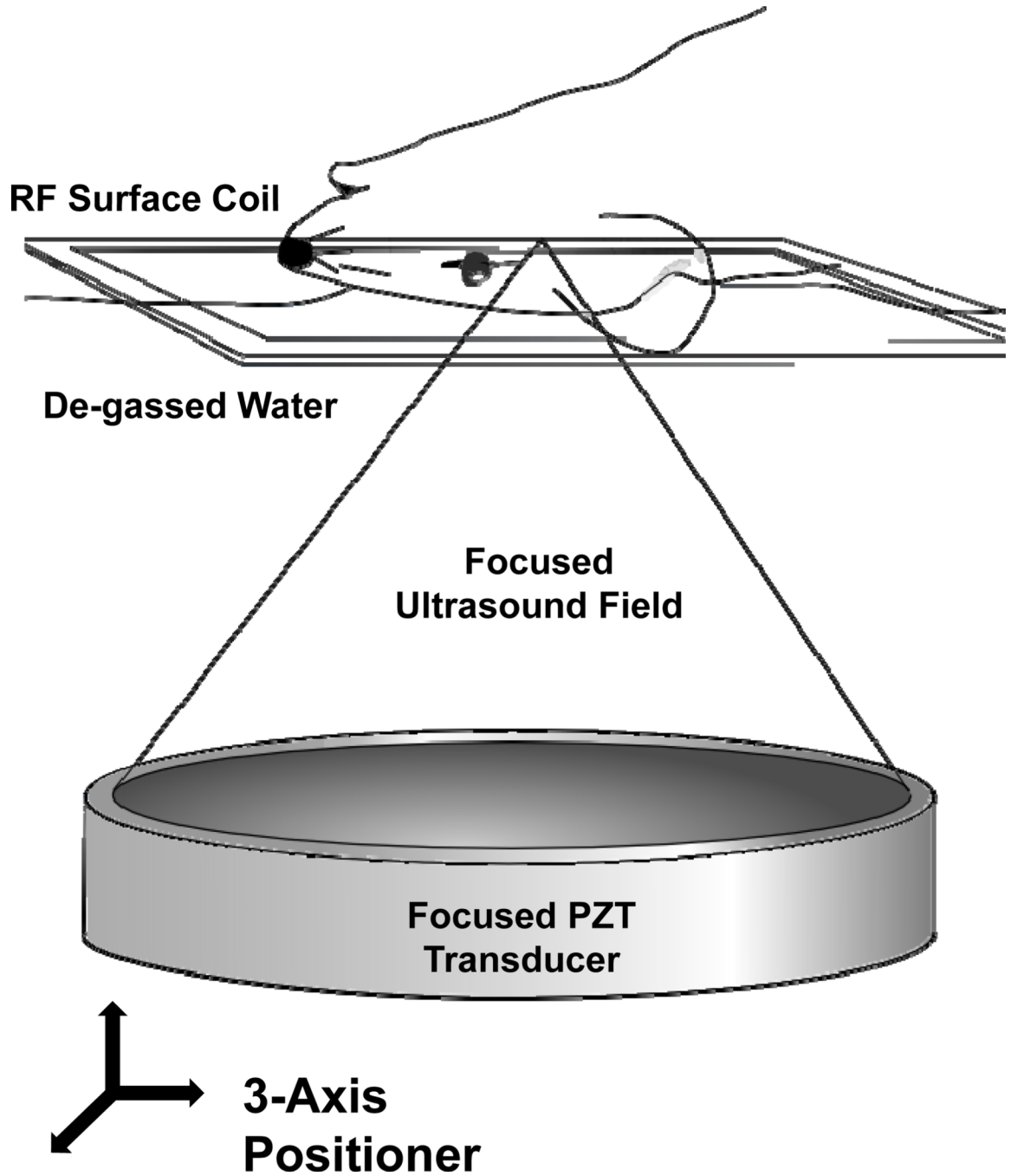
Figure 1.
The experimental MRI-guided FUS setup. The anesthetized animal was positioned supine over an MRI RF surface coil and coupled to the piezo-ceramic focused transducer through a bath of de-gassed water. The transducer was repositioned with the aid of a computer-controlled three-axis positioning system, allowing the ultrasound focus to reach any point within the brain. The entire setup fits in the bore of the 1.5T MR scanner, allowing for coordinate co-registration, targeting and confirmation of BBBD.
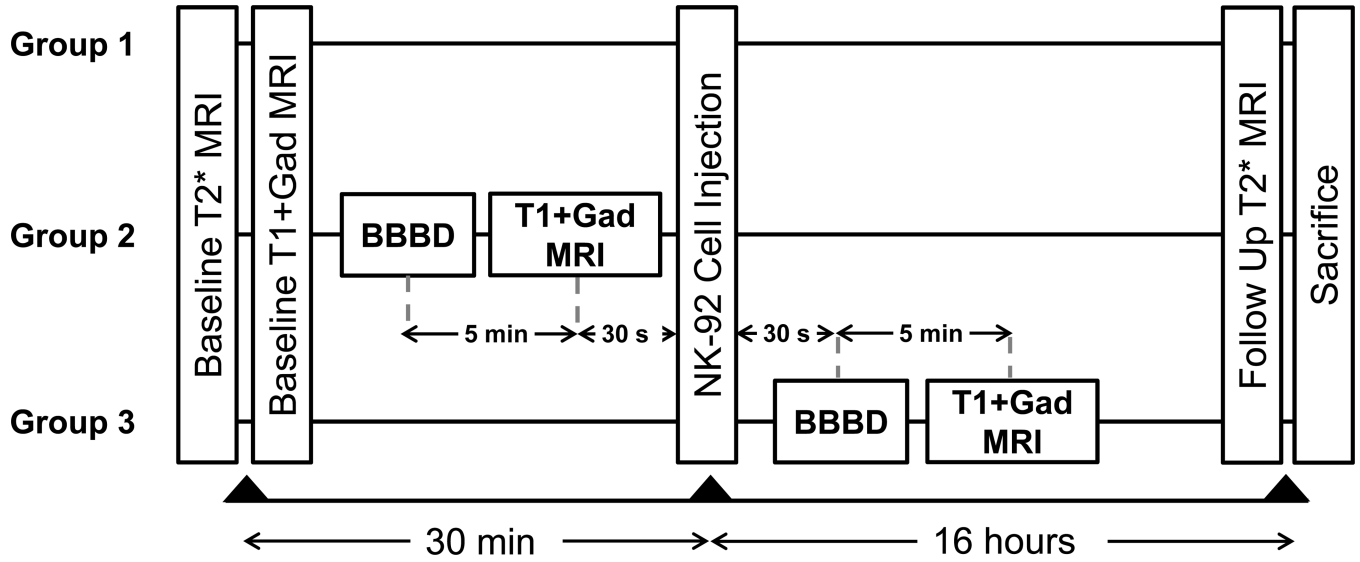
Figure 2.
Experimental timeline for the three groups. All groups initially underwent baseline imaging to assess the tumour size and location. In group 1 (control) this was followed by injection of SPIO nanoparticle labeled HER2-specific NK-92 cells. Follow-up imaging was performed at 16 hours following cell injection and immediately prior to sacrifice. Group 2 underwent BBBD, followed 5 minutes later by T1-weighted MRI with contrast to assess the change in contrast extravasation. Cells were then injected approximately 30 s after the completion of the imaging. In group 3, cells were injected via the tail vein and BBBD initiated 30 s after the injection. T1-weighted MRI was performed 5 minutes post-BBBD again to assess the change in contrast extravasation. Both groups 2 and 3 were imaged at 16 hours following the cell injection and immediately euthanized.
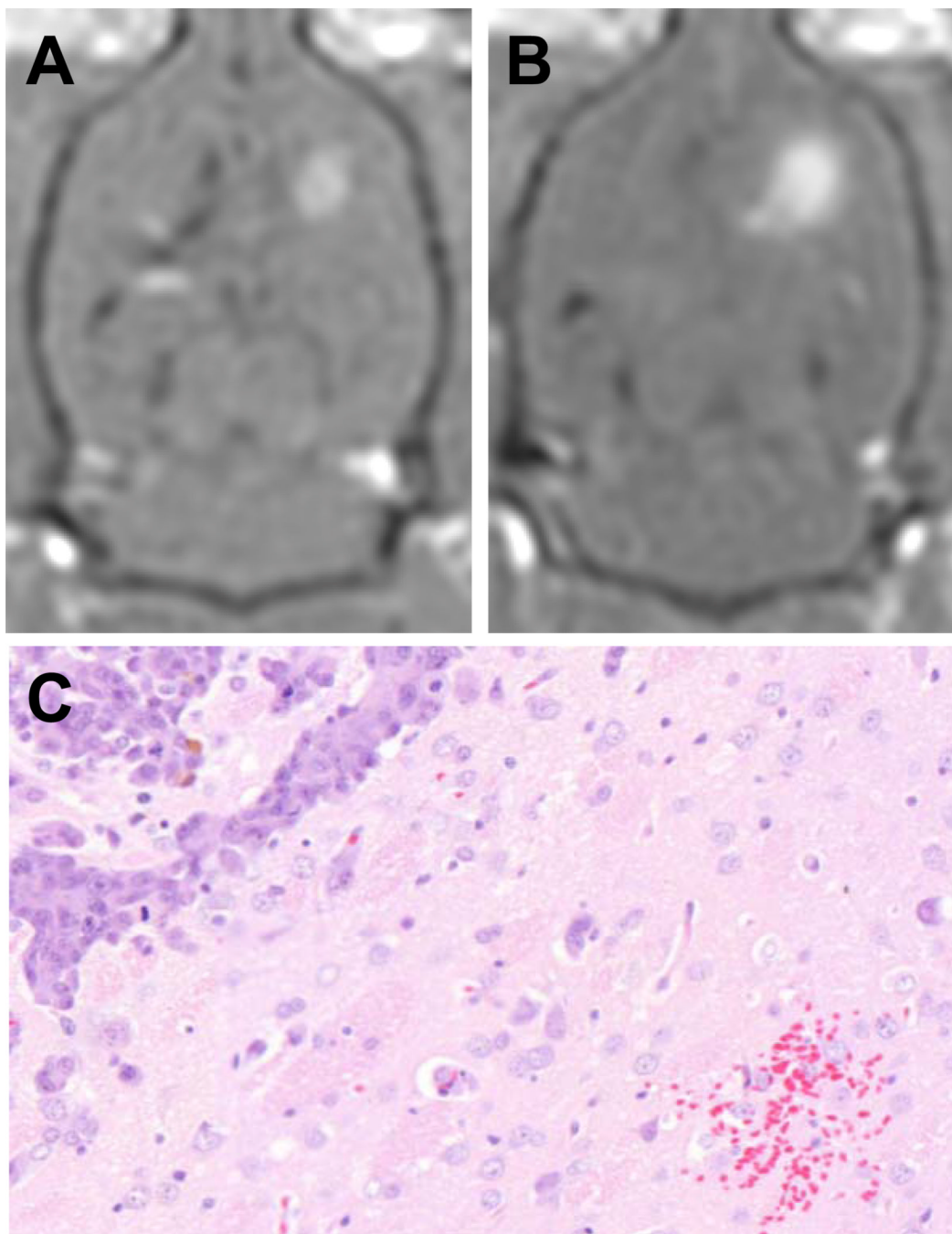
Figure 3.
The results of blood-brain barrier disruption with FUS. Representative T1-weighted MR images with Omniscan contrast of the tumor before and after BBBD, A and B respectively. The average enhancement of untreated tumors was 17 ± 8 % but increased to 34 ± 10 % following exposure to ultrasound and microbubbles (mean $\pm$ SD, $p<0.05$). A small region of erythrocyte extravasation was seen in one of the treatment animals, C. There was no further evidence of tissue injury.
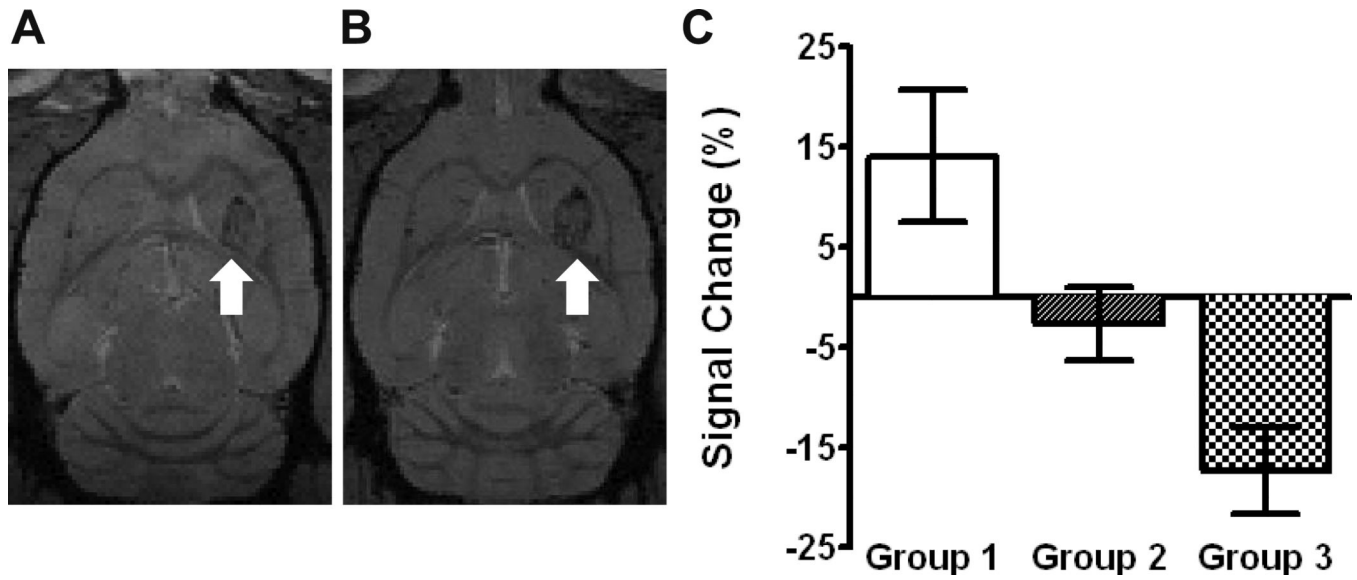
Figure 4.
HER2-specific NK-92 cell detection with 7T MRI. A baseline axial T2*-weighted MR image from group 3 is shown with the tumor identified in the left frontal striatum (white arrow), A. The corresponding post-treatment image demonstrates a signal reduction at the tumor site (white arrow), B. C shows the average signal intensity change (mean ± SEM) at the tumor site following treatment. A negative change suggests the accumulation of iron-labelled effector cells. There was a statistically significant difference between group 3 and group 1.
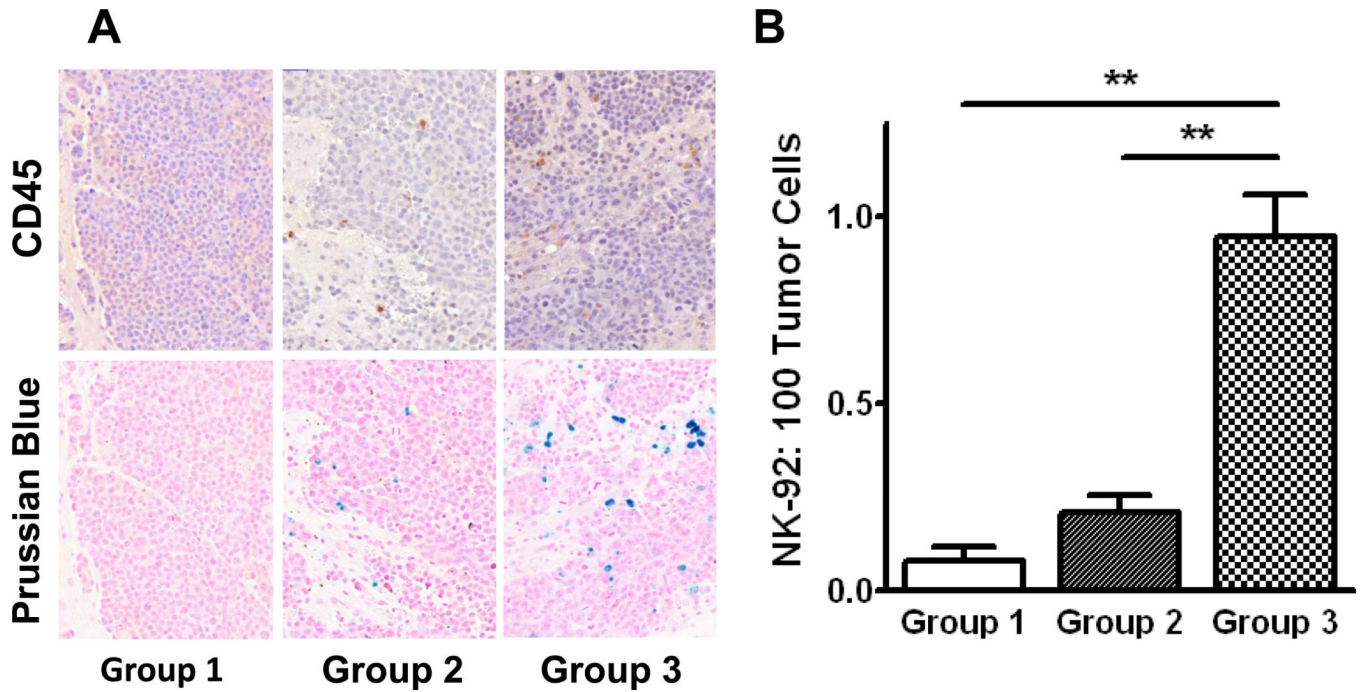
Figure 5.
Histological quantification of HER2-specific NK-92 cells accumulating at the tumor site. Effector cells were co-localized with CD45 IHC (upper panel) and Prussian blue histochemistry (lower panel) in the three experimental groups, A. HER2-specific NK-92 cells reaching the tumor were quantitatively assessed (mean ± SEM), B. When NK-92 cells were injected prior to BBBD, the number reaching the tumor was significantly higher than if they were injected following or without BBBD (group 3 vs groups 1 and 2: 0.95 ± 0.23 vs 0.09 ± 0.11, 0.21 ± 0.15, $p < 0.01$). There was no statistical difference between groups 1 and 2. These results are in agreement with the iron-sensitive MR imaging in Figure 4.
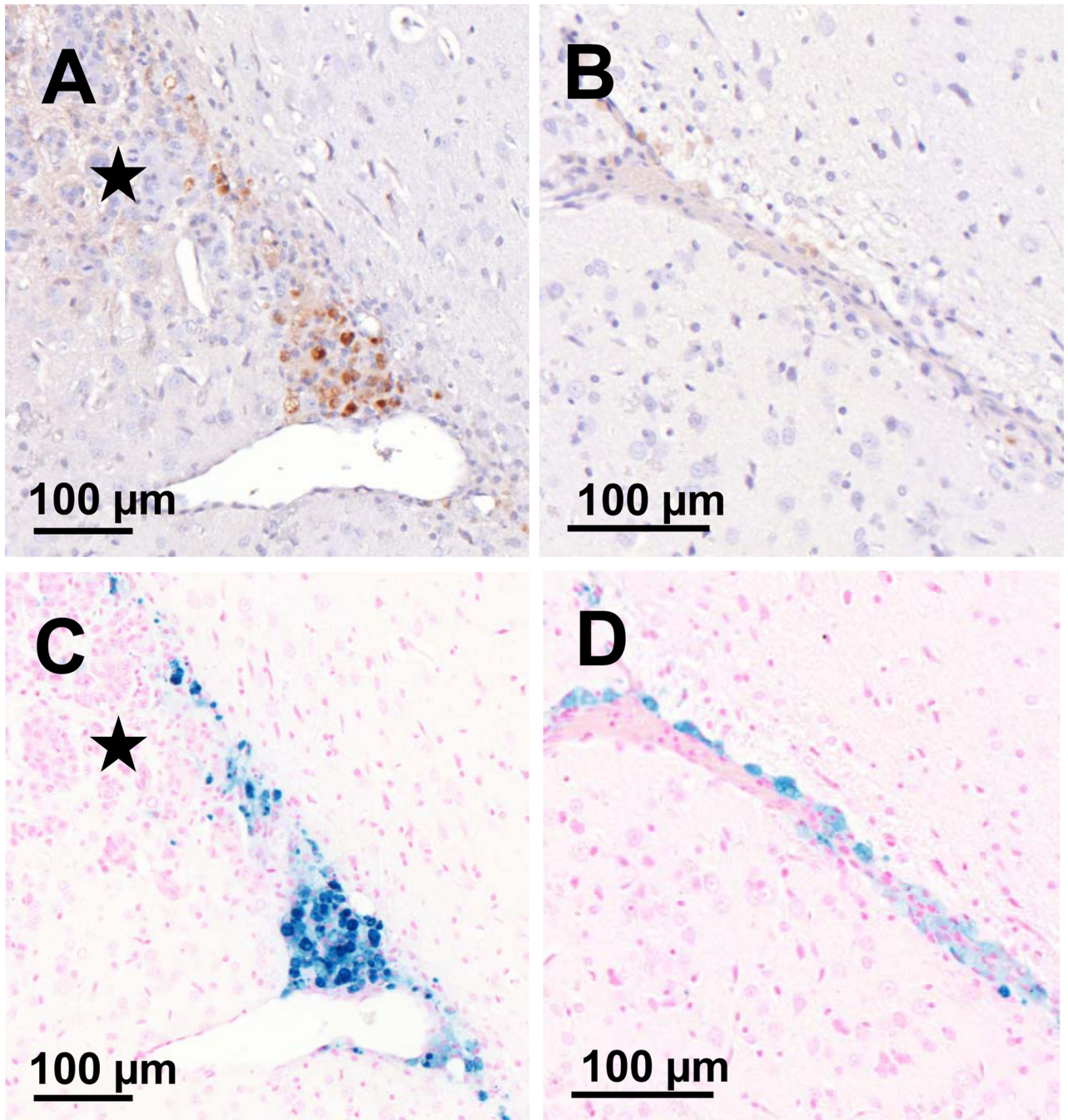
Figure 6.
FUS causes the translocation of HER2-specific NK-92 cells from the vasculature into the brain and tumor when they are present in the circulation at the time of BBBD. A, CD45 IHC depicting a vessel from which a large number of cells have extravasated and appear to track to the tumor (indicated by the star). B, the corresponding Prussian blue stained section is shown, colocalizing the HER2-specific NK-92 cells. C, a normal capillary adjacent the tumor but within the sonicated region, shows HER2-specific NK-92 cells forced to the adluminal surface of the vessel. FUS results in HER2-specific NK-92 cells circumventing both the BBB and BTB. D, the corresponding Prussian blue section. These cell distributions were seen exclusively in group 3 animals.
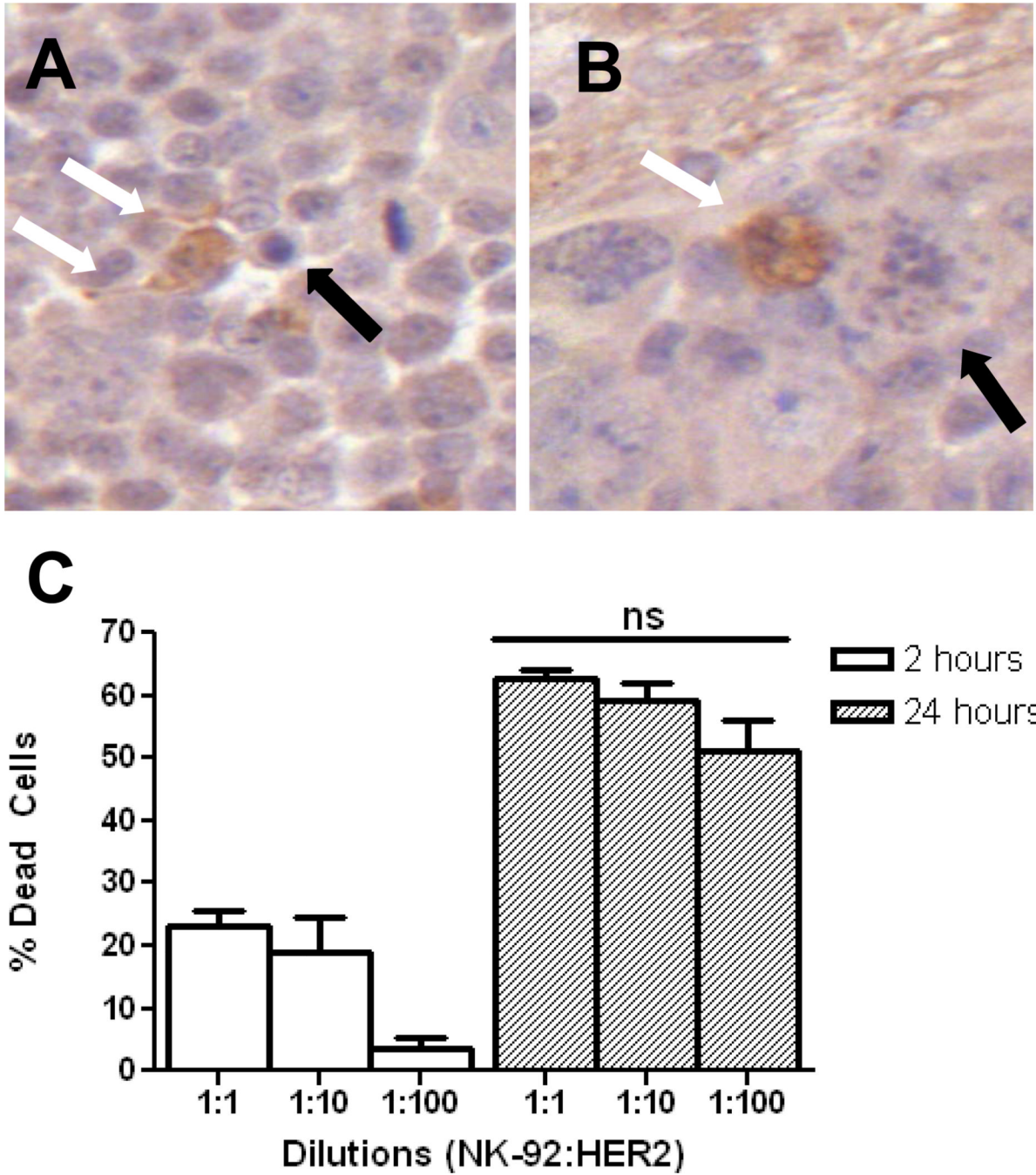
Figure 7.
HER2-specific NK-92 cells accumulate at the tumor and have preserved function. A, IHC for granzyme B highlights an NK-92 cell releasing granzyme B into the surrounding extra-cellular space (white arrows). An adjacent apoptotic tumor cell can be seen (black arrow). B, granzyme B-containing NK-92 cell (white arrow) causing apoptosis in a tumor cell (black arrow). At 24 hrs, a 1:100 ratio of effector:tumor cells is statistically no different (p > 0.05) in causing tumor cell lysis than higher starting ratios, C. This is the ratio of effector-to-tumor cells that was achieved *in vivo* in group 3.